LEO satellite imaging with adaptive optics and marginalized blind deconvolution

Cyril Petit, Laurent Mugnier, Aurélie Bonnefois, Jean-Marc Conan, Thierry Fusco, N Levraud, Serge Meimon, Vincent Michau, Joseph Montri, Nicolas Vedrenne, et al.

LEO satellite imaging with adaptive optics and marginalized blind deconvolution

C. Petit
DOTA/Onera, Paris Saclay University, 92322 Châtillon, France

L. Mugnier, A. Bonnefois, J.-M. Conan, T. Fusco, N. Levraud, S. Meimon, V. Michau, J. Montri, N. Vedrenne, M.-T. Velluet
DOTA/Onera, Paris Saclay University, 92322 Châtillon, France

R. Fétick
DOTA/Onera, Paris Saclay University, 92322 Châtillon, France
Aix Marseille University, CNRS, CNES, LAM, Marseille France

ABSTRACT

Space Situational Awareness has become a key issue both for defense and civilian/industrial applications. Identification of potential or active threats and monitoring of key assets and operations are at stake. This activity also includes the follow up of dedicated satellites (such as telecommunication, observation), traffic handling, debris identification and tracking. We present current work performed at Onera on Adaptive Optics (AO) for Low Earth Orbit (LEO) satellite imaging. We describe briefly our AO system and its performance. We also address recent developments on image post-processing based on marginalized blind deconvolution combined to parsimonious PSF modelling. Finally, we present on sky results.

1. INTRODUCTION

Recent announcements emanating for instance from the United States of America or France, have shown that space is now an explicit part of national defense strategies. As such, monitoring of key assets, control of operations such as satellite posting and identification of potential or active threats are required, from Low Earth Orbit (LEO) to Geosynchronous Earth Orbit (GEO) orbits. These issues not only matter for National Defense. It may also be of particular interest for civilian applications, such as monitoring of dedicated satellites (telecommunication, observation, and scientific missions), traffic handling, debris identification and tracking. LEO orbits are particularly concerned with an increasing number of satellites occupying this space. Trajectories can be easily tracked thanks to radar detection, while radar imaging can provide identification of satellites, though with limited resolution and in-depth imaging [1]. Optical imaging can provide complementary high resolution images and assessment of the identity, status, dynamics of a satellite and control of its vicinity. This requires large aperture telescopes with fast steering capabilities to track fast moving targets. Adaptive Optics (AO) is then required to compensate for atmospheric turbulence. The USA has thus developed state-of-the-art assets in this prospect [2][3]. The goal of this paper is to present and discuss the results obtained with a dedicated prototype. We also present innovative work for image post-processing in this particular framework.

Onera has indeed developed for the French Defense Agency a prototype of Adaptive Optics (AO) assisted imager of LEO satellites. This system has also been exploited to demonstrate LEO satellite-to-ground optical telecommunications [4]. Indeed, LEO satellite space-to-ground optical telecommunication faces similar issues for both tracking and compensation for turbulence with AO, on similar targets. The AO bench is located on the MeO telescope of the Observatoire de la Cote d'Azur (OCA) Considering LEO satellite imaging, or optical telecommunication, the performance is strongly dependent on the fast temporal evolution of turbulence, driven by the satellite slew rate. We have thus developed a GPU-CPU based real time controller to reduce loop delay and thus temporal error. This controller also provides the flexibility to support the implementation of partial automation as an answer to fast evolving conditions. Considering satellite imaging, post-processing is also a key issue. We have thus developed dedicated blind deconvolution algorithms taking advantage of recent work performed in astronomy and biomedical imaging [5][6][7][8]. We first describe briefly the AO set-up. We discuss system requirements and AO system design trade-offs. We then discuss post-processing and present current results obtained on civilian LEO satellites.

2. METHODS AND MATERIALS

The AO system, called ODISSEE, is located on the MeO telescope of OCA that belongs to the French National Centre for Scientific Research (CNRS). The combined use of ODISSEE and the MeO telescope is the result of a fruitful collaboration with CNRS, for space observation and optical telecommunication. The MeO telescope and the AO system have been partly described in the framework of tests for satellite-to-ground optical telecommunication [4]. We summarize the main features and limitations of the set-up.

Experimental set-up

The MeO station is a versatile telescope located in the hinterland of Grasse, in the south of France, at an altitude of 1270 meters, up to now mostly used for artificial satellites and lunar laser ranging. This 1.5-meter telescope (Fig. 1) is installed on an Alt-Az mount allowing target tracking up to 5°/s, with a better than 20" Peak-Valley (PV) pointing accuracy thanks to a two-stage dedicated tracking loop. These features make this telescope a very good candidate for various research programs such as optical time transfer, adaptive optics, high resolution imaging, debris detection, optical telecom and astronomical observation.

Fig. 1 Picture of MeO telescope**.**

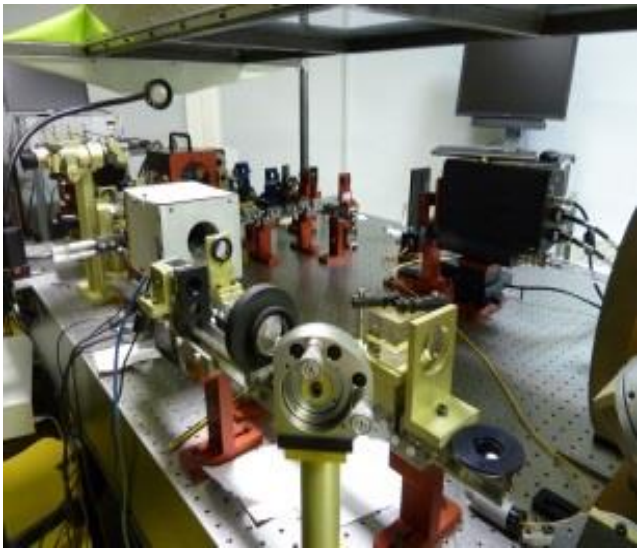

Fig. 2 Picture of ODISSEE AO bench**.**

The ODISSEE AO bench (Fig. 2) has been designed and integrated by ONERA at the coudé focus of MeO for investigation of various applications, including visible imaging. In this prospect, it has been adapted from an existing laboratory AO bench, favoring versatility rather than performance. As a consequence, this AO system provides a useful tool to assess propagation conditions and the performance of new concepts, and to investigate the limitations of AO for imaging applications.
The light from MeO coudé focus enters the bench at the bottom-right of the image. The AO bench includes a pupil derotator, an atmospheric dispersion compensator, a pupil stabilizer, a fast tip/tilt mirror to compensate for atmospheric turbulent tip/tilt, pointing residuals and vibrations, an 88 actuator deformable mirror, a Shack-Hartmann based wavefront sensor and an imaging camera.
ODISSEE uses a visible Shack-Hartmann WaveFront Sensor (SH-WFS) with 8x8 square sub-apertures. The WFS camera is a First Light Imaging OCAM² camera (Electron Multiplying Charge Coupled Device--EMCCD) with an E2V chip of 240x240 pixels. Slopes and intensities per subaperture are recorded with a frame rate of 1500 Hz. High order correction is performed thanks to a CILAS piezo-stacked Deformable Mirror (DM) with 88 actuators (10x10 cartesian grid). It provides a +/-5 µm mechanical stroke and exhibits a 10 kHz bandwidth.
The AO loop is controlled thanks to a Linux Personal Computer (PC) Real-Time Controller (RTC), developed by Shakti Company, implementing various possible features both in terms of wavefront sensing and control algorithms.
The internal performance of the AO bench in this configuration (defined as Strehl Ratio of a non-resolved source at the entrance focus) is 88% at 850 nm (representing the ultimate performance of the system on sky), due to residual aberrations (high order residuals and non-common path aberrations).

System requirements and limitations

The ODISSEE AO bench is a prototype and as such, is the result of a complex trade-off. The main drivers for this experiment is to be able to investigate AO performance and automating as well as image post-processing on various targets, considering possibly faint targets. High system availability, in most turbulence conditions, and on most targets has not been considered so far. We discuss here this trade-off. The following discussion is obviously not an exhaustive system analysis that should be performed considering population of desired targets, their characteristics and trajectories, local statistics of turbulence etc. The basic idea is to underline in simple conditions and straightforward analysis the key features that have been the drivers for the current system trade-off.
To better understand the system requirements for satellite imaging, and the AO bench design, it is interesting to consider the evolution of integrated parameters such as r_0 or greenwood frequency f_G along an observation. We assume a 1.5m telescope and observation at some 850nm, value we considered as an acceptable compromise between residual turbulence level, flux and resolution. We consider in the following a satellite at 700 km altitude, assuming a circular orbit. For the sake of simplicity, we assume also a 90° maximum elevation without loss of generality. We consider an ITU turbulence profile, relevant for nighttime observation proposed in Fig. 3. This profile leads to a 1.2'' seeing at zenith, rather common during observations at OCA (seeing usually larger than 1'' [9]).
As it is difficult to consider relevant hypothesis for wind profile, both in terms of amplitude and direction, we assume no natural wind, and focus on the sole contribution of apparent wind speed related to satellite evolution (that evolves linearly with altitude along the line of sight, depending on the telescope slew rate). Considering the very high velocity in altitude induced by slew rate this assumption can be considered as relevant, except close to the ground. We can then evaluate the evolution of distance, r_0 (at 500nm), Greenwood frequency f_G and the related characteristic time $\tau_0 = 0.314/f_G$. These terms are plotted in Fig. 4 as a function of the elevation angle.
As can be seen on Fig. 4, distance of the satellite to the ground as well as r_0 evolve quickly by a factor 3 between 10° and 90° elevation. However, their evolution can be considered as smoother beyond 40°. In other words, flux and seeing conditions will be much more stable beyond 40°. Similarly, although the slew rate is highest at zenith and drops below, the Greenwood frequency and associated τ_0 remain rather stable between 40° and 90° elevation. They quickly evolve below 20° elevation. But on the whole f_G can be considered as stable beyond 40° to 120Hz and τ_0 lower than 1.5ms. These values however are quite demanding.
We consider here a simplified estimation of error budget, for a 1.5m telescope, based on the previous turbulence profile, assuming the 1.2'' seeing and a wind profile driven by satellite tracking. We assess the evolution of the various terms of the error budget with respect to the number of linear actuators and AO bandwidth (or cut-off frequency), for a 60° line of sight first, then discuss noise contribution depending on target apparent magnitude and system parameters.

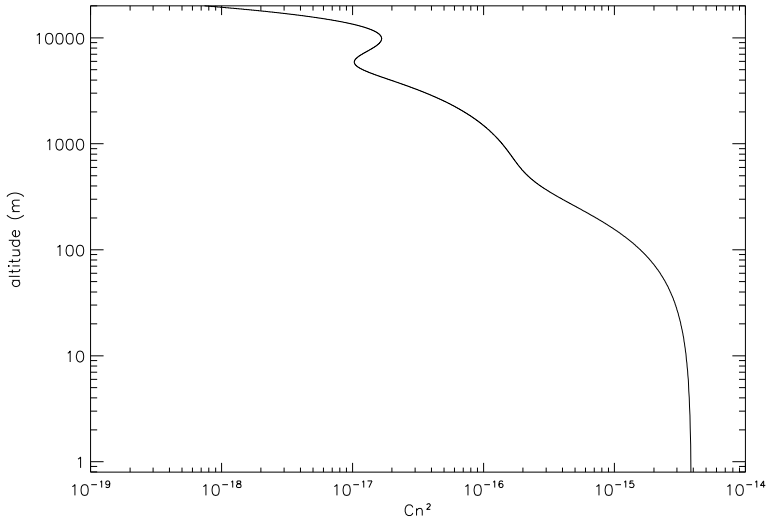

Fig. 3 ITU turbulence profile considered.

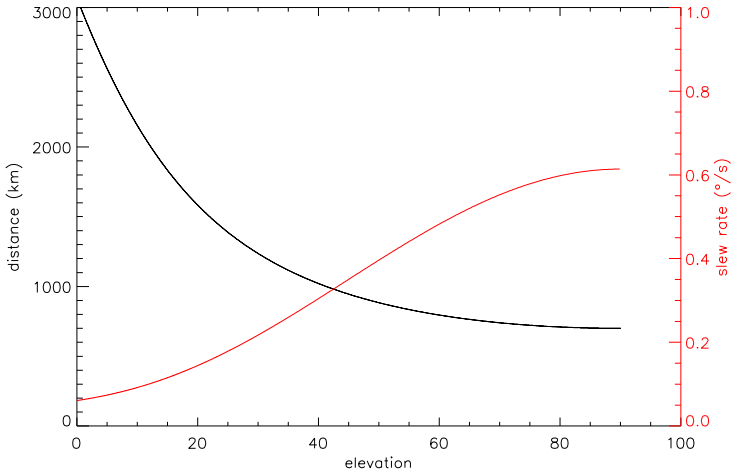

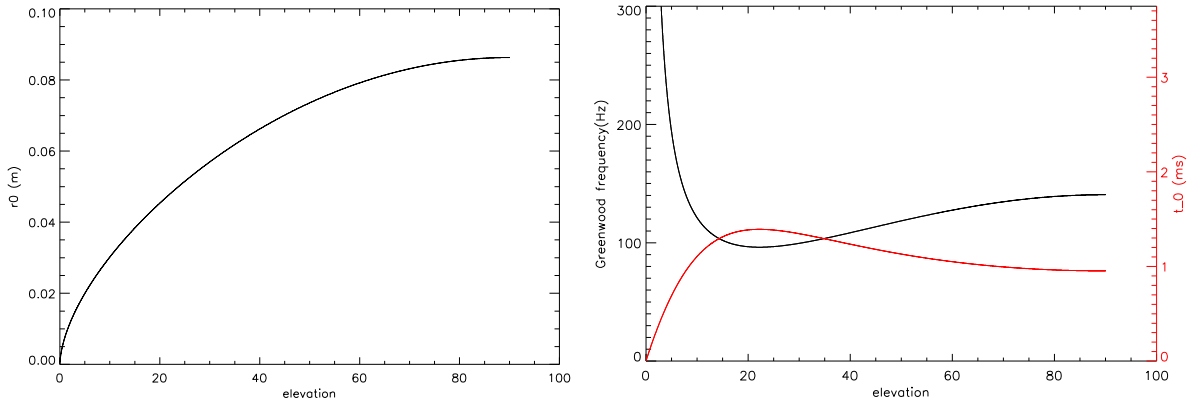

Fig. 4 Evolution of distance and slew rate (top), $\mathbf{r_0}$ (bottom left), and $\boldsymbol{f_G}$ and $\boldsymbol{\tau_0}$ (bottom right) along satellite tracking at 850nm.

As can be seen in Fig. 5, the contribution of the temporal error is dominant as long as the AO bandwidth is not higher than 100Hz for small systems (in terms of linear actuators across the pupil) and 200Hz for larger ones, which means

sampling frequencies typically higher than 1500Hz and 3 kHz respectively (for a 2 frame overall delay), which is consistent with τ_0. Global evolution of the curves with elevation mainly follows the one of r_0 as evolution of the temporal characteristics of turbulence is almost insignificant down to 20°.

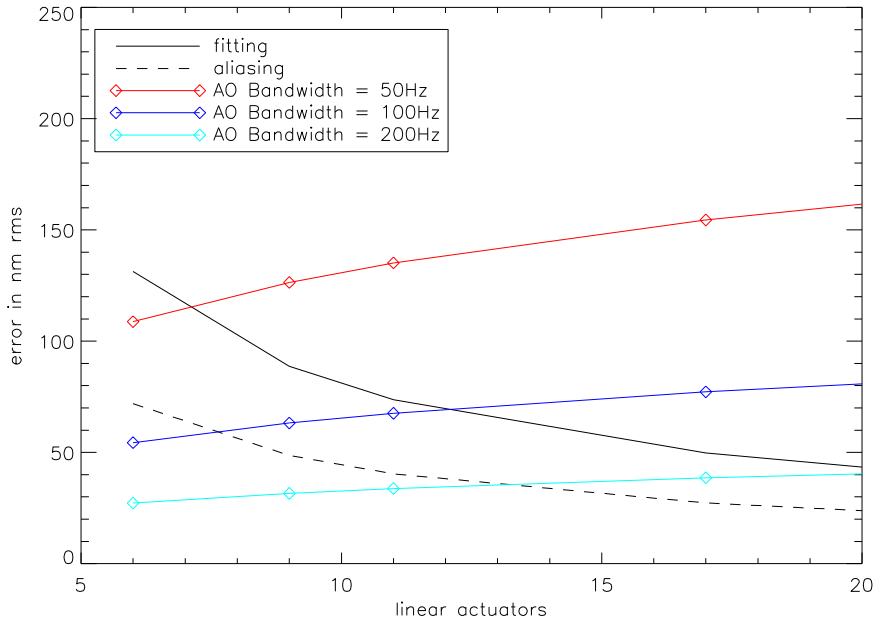

Fig. 5 Evolution of fitting, aliasing and temporal error with number of linear actuators and AO Cut-Off Frequency at 60° elevation**.**

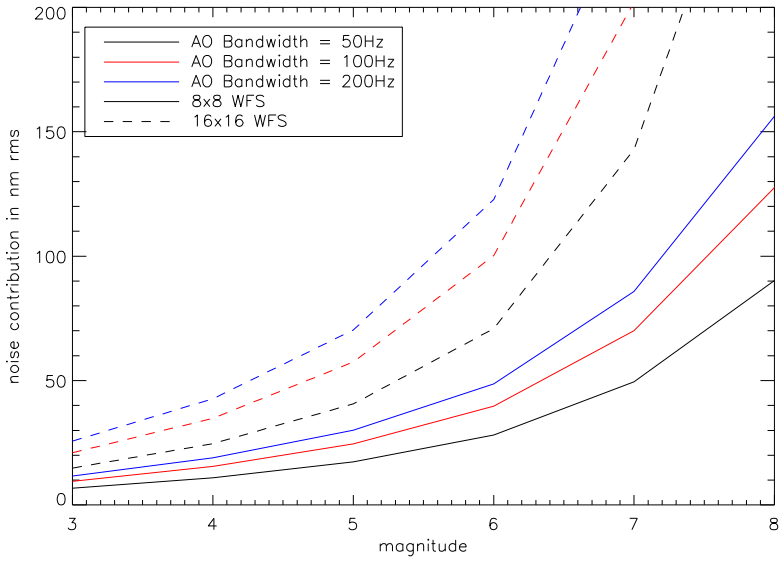

Fig. 6 Evolution of noise contribution to the error budget depending on AO configuration (2 cases) and AO Cut-Off Frequency**.**

We now consider noise propagation on the AO system performance. Such analysis may be difficult considering the variability of targets, their inner reflectivity and orientation. For the sake of simplicity the target is assumed here to be a sphere, with an apparent integrated magnitude given in V band. We account for the atmospheric transmission as well as spectral transmission of the system that could clearly be improved. We consider a slightly resolved satellite

(at WFS level) at 700km and account for the WFS characteristics (noise, wavefront sensing algorithm, exposure time) assuming a fix sampling whatever the configuration for relevant comparison.
Fig. 6 shows the evolution of WFS noise propagation through the AO loop and associated contribution to the error budget for the three AO bandwidths and two system configurations, for the same 60° elevation. While the noise contribution is slightly affected by AO loop bandwidth, it significantly evolves with system configuration due to increase of the number of sub-apertures.
Same analysis can be carried out for various elevations, and shows a degradation when going to low elevation, due to increased distance to the satellite, but while the result is hardly affected by AO bandwidth, it is strongly dependant from the number of degrees of freedom of the system.
This very simple analysis of the error budget clearly shows that considering our main drivers, the temporal error is clearly a show-stopper that shall be dealt with prior to any increase of the number of degrees of freedom, as the temporal error and noise contribution will strongly increase with the number of measured and corrected modes.
As a result, most of our efforts have been focused on accelerating the AO loop. In order to reduce the temporal error, a GPU-CPU based RTC has been developed with the Shakti Company. This evolution leads to a drastic reduction of computation time, through a cost effective and simple software implementation as discussed in [10] and tested for instance in [11]. Our implementation allows to directly transferring the pixels from the OCAM² camera to the GPU, through a Matrox frame grabber. All wavefront sensing computations are performed by the GPU, while control and system optimization are performed by the CPU. An NVIDIA GeForce 1060 GPU board has been used combined to low latency Ubuntu operating system. As a result a 2.2 frame overall loop delay at 1.5 kHz is obtained (70µs RTC pure delay), leading to almost 100Hz cut off frequency. This extended cut-off frequency also benefits to vibration filtering, as clear vibrations have been identified in the system, induced by telescope tracking, leading mostly to a 50Hz contribution, now dampened. This first implementation still allows significant additional gains in the future, as the GPU board is weakly used and computation pipeline can be significantly improved.
This fast real-time pipeline also allows introducing partial automation of the AO loop. Conditions strongly evolve along the observation: slew rate and SNR due to satellite distance, turbulent profile and thus apparent seeing due to elevation. For all these reasons, the AO loop optimal parameters should evolve rather quickly, without human real time intervention. The gain in real time control delay has allowed us to implement background and noise automatic follow up, as well as automatic target detection. The Shack-Hartmann wavefront sensing optimization has been fully automated, including the online adjustment of EMCCD gain. An adaptive control is now considered.
Finally, though the system has been designed to address faint objects, the performance is limited by the optical system transmission, which was initially limited to only 10% throughout the overall system. This limitation is currently being dealt with.

Post-Processing

Our system requirements, as well as the previous analysis, lead to an AO system mostly working in partial correction. In these conditions, images post-processing becomes critical and must rely on highly efficient and robust algorithms to restore the object in spite of turbulence residuals and noise.

In LEO satellite imaging as in many imaging modalities, the image can be modelled as the noisy convolution of the sought object with a PSF that is unknown, both because a recorded star image would bear little resemblance with the actual PSF of a fast-moving satellite and because the WFS measurements would yield a noisy and low-resolution version of the actual PSF. The conventional way of tackling this lack of knowledge is to perform a “blind” or “myopic” deconvolution, consisting in a joint estimation of the sought object and of the PSF, if possible with additional constraints such as PSF band-limitedness and positivity, object positivity and support, etc (see [12] for a review). Without positivity or object support constraints the blind deconvolution has been shown to be degenerate for a quadratic regularization [5], in the sense that the estimation leads to a wrong (object, PSF) couple even if the noise level is arbitrarily small. We have recently checked that even with the positivity constraint and a non-quadratic regularization, the problem remains degenerate in practice [6].

The problem fundamentally lies in the fact that there are too many unknowns for too little data, and the idea for a solution is twofold. Firstly, we use a parsimonious PSF model tailored for AO-corrected PSFs in order to reduce the number of unknowns [7]. Secondly, we identify the PSF by “estimating the PSF only”, on average for all possible objects within a given class. This idea of estimating only the PSF is embodied in the so-called *marginal blind deconvolution*. The marginal approach drastically reduces the number of unknowns by integrating the object out of the problem. Our approach relies on method [5] called AMIRAL (Automatic Myopic Image restoration Algorithm),

where the likelihood is marginalized over the unknown object (of a given Power Spectral Density (PSD)), and maximized as a function of the sole PSF. Then we deconvolve the image in a non-blind fashion by a positively constrained Maximum A Posteriori (MAP) method with the PSF thus identified. Fig. 7 shows the workflow of the whole procedure.

Additionally, in this communication, we explore the possibility of combining the marginal blind deconvolution outlined above, with a positivity constraint on the object *during* the PSF identification. . The marginal approach usually integrate the object out of the problem under the hypothesis of a Gaussian prior probability density function, and thus without a positivity constraint on the object. By exploiting the remarkable identity that links the joint and the marginal log-likelihoods (see Eq. 18 of [8]), we were able to impose a positivity constraint on the object within the marginalized PSF identification, in order to improve the latter and, in turn, the restored object.

Finally, because the PSDs of the object and of the noise are actually unknown, we must also estimate them. To this purpose, we also use a sparse parameterization for the object's PSD with only three parameters [13], so that the statistical contrast of our estimation (ratio of number of data over the number of unknowns) remains much greater than unity, and the appealing theoretical properties of Maximum Likelihood estimation such as consistency are retained in practice.

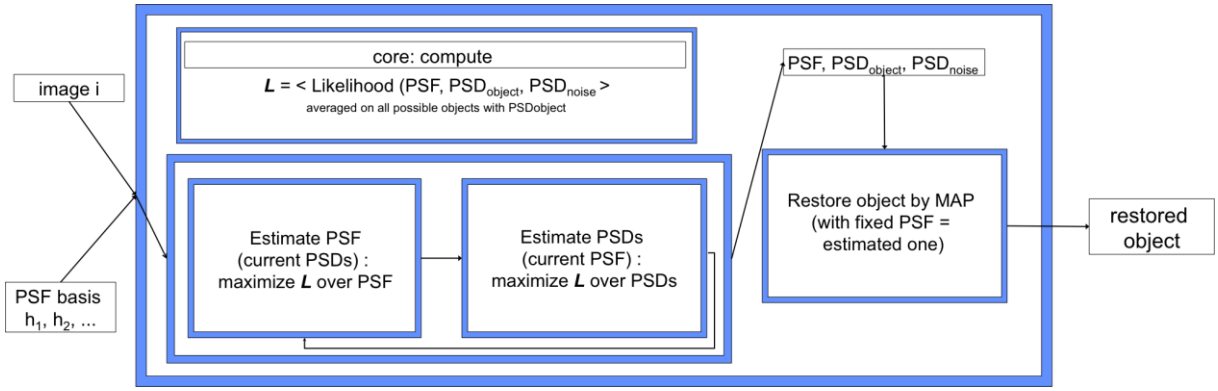

Fig. 7 Sketch of the deconvolution procedure

3. RESULTS

Although the analysis of on-sky performance will not be detailed here, some experimental images with AO correction are shown. The imaging of the ENVISAT satellite has been performed with the system set up on the MeO telescope and is presented below. ENVISAT (Fig. 8) is an ESA satellite, launched in 2002, and dedicated to Earth observation through radar and spectrometry. This is a large satellite (26 m long with its solar panels) evolving at some 800km altitude. However, this satellite is no more controlled, since 2012, and represents today the largest space debris in orbit. It has been observed by CNES through the Pleiades space telescope and by TIRA Inverse Synthetic Aperture Radar imager (Fraunhofer institute) [1] in order to provide a long-term analysis of the satellite rotation in the prospect of a possible de-orbitation program led by ESA.

Fig. 8 Picture of ENVISAT

Fig. 9 shows AO corrected images of ENVISAT taken from a sequence of a few minutes. The satellite rotation is clearly visible along the sequence, thanks to the diffraction limited images, as illustrated in these few snapshots, as well as some structural details.

The application of post-processing can then help restore the object and significantly increase the image quality as shown in Fig. 10. Here the marginal blind deconvolution of [5], AMIRAL, has been applied, i.e. the PSF identification is performed without positivity constraint, then the object is restored with the identified PSF and a positivity constraint. These images can be compared to ISAR images as shown in [1], or to CAD images as proposed in Fig. 11.

Preliminary results of a restoration obtained with the object positivity constraint imposed within the PSF identification are shown in Fig. 12. These results have been obtained on the first image of the series proposed in Fig. 9 to Fig. 10. One can note a slight improvement of the object thanks to this constraint, considering reduction of residual high frequencies while preserving sharp edges.

As images sequences are obtained on a few hertz time basis, it is also possible to evaluate, so far through simple image correlation, the satellite tumbling period. Basic image registration leads to an estimation of 202s tumbling period. This value can be compared to the results of the detailed analysis performed through satellite laser ranging in 2013 [14]. A 134.7s tumbling period was then evaluated, with an increase of this tumbling period estimated to 36.7ms per day. These values lead to an estimated period of 206.9s at the time of the acquisition of these images, assuming constant increase of the tumbling period. While these numbers are coherent, the goal is not of course here to try to compare with the accurate measurements performed with satellite laser ranging. A single sequence is considered here, with very simple image correlation. In addition, many biases are not considered such as apparent rotation of the satellite with respect to ground station. This result only shows that satellite imaging can provide interesting information, in particular when benefitting from enhanced image quality.

A second illustration comes from the observation of the MICROSCOPE satellite. MICROSCOPE is a micro-satellite program led by Cnes, involving Onera, OCA and Zarm, dedicated to the verification of the equivalence principle. MICROSCOPE is a small satellite of $2m^3$ at some 700km altitude, a sketch of the satellite is provided Fig. 13. The payload T-Sage was developed by Onera. The program ended in 2018. To reduce the deorbitation time and space debris, the passive deorbiting system IDEAS (Innovative DEorbiting Aerobrake System) was used. It consists in two deployable arms based on thin aluminum foil filled with nitrogen (Fig. 13). In addition, these arms are equipped with two sails of 4m long each to increase the surface. These arms provide a dragging force to accelerate deorbiting. Correct inflation of the wings was a key issue. Fraunhofer institute provided remarkable images with its space radar TIRA, confirming the deployment of the wings [15].

Images of MICROSCOPE were obtained with ODISSEE, in spite of the small size of the target, and in difficult seeing conditions considering the limitations of the bench. Fig. 13 shows one image taken from the sequence acquired with the set-up, showing clearly the inflated wings. This shows promising possibilities even with limited AO performance.

Fig. 9 Series of AO corrected images of ENVISAT.

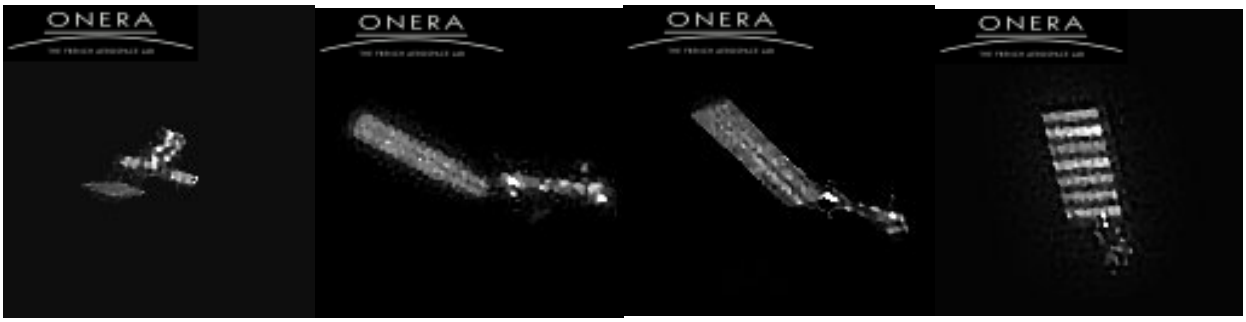

Fig. 10 Series of AO corrected images of ENVISAT, after post-processing.

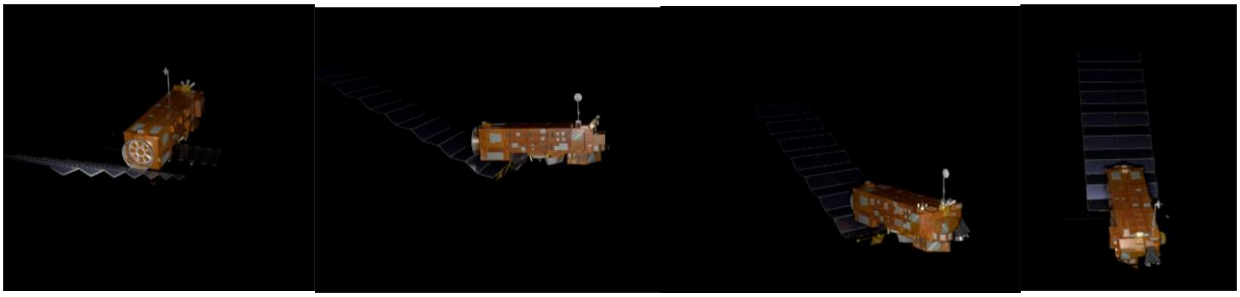

Fig. 11 Series of CAD images of ENVISAT, in similar orientations.

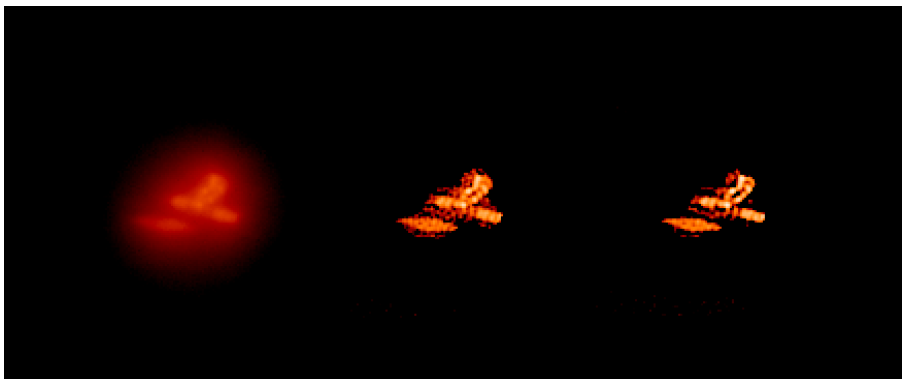

Fig. 12 Left: raw image; center: blindly restored image with AMIRAL; right: blindly restored image with an object positivity constraint within the PSF identification. All images in false color (with the "heat" LUT) to bring out low light level details.

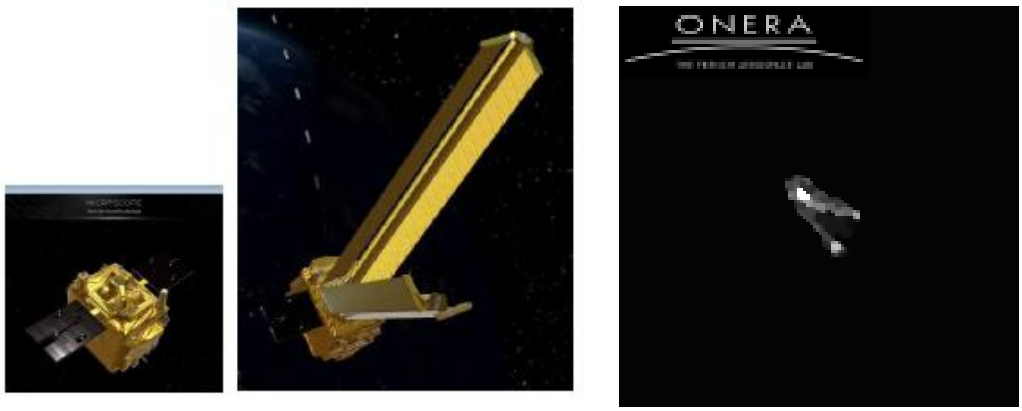

Fig. 13 Left: sketches of MICROSCOPE with and without inflated wings. Right: post-processed image obtained with ODISSEE.

4. CONCLUSION

We have developed an AO system prototype for LEO satellite imaging. Our main drivers (limited complexity, access to faint target, investigation of AO performance and automating) have led to a simple system for which temporal error is a main driver. The optimization of the real-time computation pipeline has allowed to drastically improve the final AO performance and meet these main requirements. This system represents a key asset for LEO imaging but also for optical telecommunications investigation, so as to deal with fast evolving conditions through automated systems. Technological developments shall be pursued further, as telecommunication applications tend to push sampling frequencies higher, with 5 to 10 kHz goals. In the meantime, refining AO loop control, considering for instance predictive solutions based on Linear Quadratic Gaussian Control, could participate to the reduction of temporal error such as in [16]. This last paper has underlined the possible gain brought by predictive control, though in particularly demanding turbulence condition. One could then wonder what is the ultimate performance that could be obtained with predictive control and its evolution with turbulent conditions and satellite characteristics. More generally, our straightforward analysis of system design shall be reconsidered for an operational system.

Post-processing of AO corrected images has also been improved, both in terms of performance and robustness, thanks to marginal blind deconvolution and use of a parsimonious PSF parametrization. Further improvements can still be expected, by taking into account the AO information as well as by processing image sequences jointly.
Next steps shall focus on increasing observation opportunities. This implies first observing at low elevations and second during daytime. Indeed, satellite imaging as well as optical telecommunications are strongly limited at low elevation, due to the strong turbulence conditions. However most of the available time of visibility of a LEO satellite is below 30°, leading to a strong reduction of observation or link duration for optical telecommunication. In addition, satellite observation is limited to a few hours in nighttime. These limitations mean considering further improvements of AO but also considering other modalities of image post-processing as underlined by [17].

ACKNOWLEGMENTS

This work has been supported by the French Defense Agency under contract 2015990015. The authors are grateful to the Shakti company for the development of the real-time computer and their strong involvement in the project. The authors are also grateful to Observatoire de la Côte d'Azur for providing access to the MeO telescope, for their extensive support and long-term involvement in this project, in particular in fine tracking of satellites.

REFERENCES

[1]. S. Lemmens, H. Krag, J. Rosebrock, I. Carnelli. Radar mappings for attitude analysis of objects in orbit, Proc. 6th European Conference on Space Debris', Darmstadt, Germany, 22-25 (ESA SP-723) (2013).

[2]. J. M. Spinhirne, Jeff G. Allen, George A. Ameer, James M. Brown, Julian C. Christou, et al.. Starfire Optical Range 3.5-m telescope adaptive optical system, Proc. SPIE 3353, Adaptive Optical, System Technologies, (1998)

[3]. L. C. Roberts, C. R. Neyman. Characterization of the AEOS Adaptive Optics System, Publications of the Astronomical Society of the Pacific, 114:1260–1266 (2002).
[4]. Petit, C, Védrenne, N., Velluet, M.-T., Michau, V., Artaud, G., Samain, E., Toyoshima. Investigation on adaptive optics performance from propagation channel characterization with the small optical transponder. M., Opt. Eng. 0001, 55(11) (2016).
[5]. L. Blanco and L. M. Mugnier. Marginal blind deconvolution of adaptive optics retinal images, Opt. Express, vol. 19, pp. 23227-23239 (2011).
[6]. R. J-L. Fétick, L. M. Mugnier, T. Fusco, and B. Neichel. Blind deconvolution in astronomy with adaptive optics: the parametric marginal approach, *Mon. Not. R. Astron. Soc.*, 496(4):4209–4220, August 2020 (2020).
[7]. R. JL. Fétick, T. Fusco, B. Neichel, L. M. Mugnier, O. Beltramo-Martin, A. Montmerle Bonnefois, C. Petit, J. Milli, J. Vernet, S. Oberti, and R. Bacon. Physics-based model of the adaptive-optics-corrected point spread function. Applications to the SPHERE/ZIMPOL and MUSE instruments, Astron. Astrophys., 628:A99 (2019).
[8]. A. Blanc, L. M. Mugnier, and J. Idier. Marginal estimation of aberrations and image restoration by use of phase diversity. J. Opt. Soc. Am. A, 20(6):1035–1045 (2003).

[9]. E. Aristidi, A. Ziad, J. Chabé, Y. Fantéi-Caujolle, C. Renaud and C. Giordano. A generalized differential image motion monitor, MNRAS 486, 915-925, doi:10.1093/mnras/stz854 (2019).
[10]. A. Sevin, D. Perret, D. Gratadour, M. Lainé, J. Brulé, and B. Le Ruyet. Enabling technologies for GPU driven adaptive optics real-time control, Proc. SPIE 9148, Adaptive Optics Systems IV, 91482G (2014).
[11]. L.F. Rodríguez Ramos, J.J. Díaz García, J.J. Fernández Valdivia,H.M. Chulani, C. Colodro Conde, J.M. Rodríguez Ramos. The use of CPU, GPU and FPGA in real-time control of adaptive optics systems, Adaptive Optics for Extremely Large Telescopes 4 Proceedings, 1(1) (2015).
[12]. L. Blanc-Féraud, L. Mugnier & A. Jalobeanu Blind Image Deconvolution, chap. 3 of Inverse Problems in Vision and 3D Tomography, pp. 97-121, ed. by A. Mohammad-Djafari, ISTE/John Wiley, London (2010).
[13]. J.-M. Conan, L. M. Mugnier, T. Fusco, V. Michau, and G. Rousset. Myopic deconvolution of adaptive optics images by use of object and point spread function power spectra, Appl. Opt., 37(21):4614–4622 (1998).
[14]. D. Kucharski, G. Kirchner, F. Koidl, C. Fan, R. Carman, C. Moore, A. Dmytrotsa, M. Ploner, G. Bianco, M. Medvedskij, A. Makeyev, G. Appleby, M. Suzuki, J.-M. Torre, Z. Zhongping, L. Grunwaldt, Q. Feng. Attitude and spin Period of Space Debris Envisat Measured by Satellite Laser Ranging. IEEE Trans. On Geoscience and Remote Sensing, vol. 52, No. 12, pp 7651-7657 (2014).
[15]. https://www.fhr.fraunhofer.de/en/businessunits/space/supporting-satellite-deorbiting-missions-with-tira.html
[16]. J. Cranney, J. De Dona, V. Korkiakoski, F. Rigaut. Identification Scheme with Stability Constraints for High Velocity Turbulence in Adaptive Optics, 2018 Australian & New-Zealand Control Conference, Swinburne University of Technology, Melbourne, Australia (2018).
[17]. M. Hart, S. Jefferies, D. Hope, J. Nagy, and R. Swindle. A Comprehensive Approach to High-Resolution Daylight Imaging for SSA, Advanced Maui Optical and Space Surveillance Technologies Conference (AMOS) (2016).